PHOTONICS Research

Low-noise 1.3 μm InAs/GaAs quantum dot laser monolithically grown on silicon

Mengya Liao,[1] Siming Chen,[1,*] Zhixin Liu,[1] Yi Wang,[2] Lalitha Ponnampalam,[1] Zichuan Zhou,[1] Jiang Wu,[1] Mingchu Tang,[1] Samuel Shutts,[3] Zizhuo Liu,[1] Peter M. Smowton,[3] Siyuan Yu,[2] Alwyn Seeds,[1] and Huiyun Liu[1]

[1]Department of Electronic and Electrical Engineering, University College London, London WC1E 7JE, UK
[2]State Key Laboratory of Optoelectronic Materials and Technologies, Sun Yat-sen University, Guangzhou 510275, China
[3]Department of Physics and Astronomy, Cardiff University, Cardiff CF24 3AA, UK
*Corresponding author: siming.chen@ucl.ac.uk

Received 8 August 2018; revised 13 September 2018; accepted 13 September 2018; posted 14 September 2018 (Doc. ID 341901); published 17 October 2018

We report low-noise, high-performance single transverse mode 1.3 μm InAs/GaAs quantum dot lasers monolithically grown on silicon (Si) using molecular beam epitaxy. The fabricated narrow-ridge-waveguide Fabry–Perot (FP) lasers have achieved a room-temperature continuous-wave (CW) threshold current of 12.5 mA and high CW temperature tolerance up to 90°C. An ultra-low relative intensity noise of less than −150 dB/Hz is measured in the 4–16 GHz range. Using this low-noise Si-based laser, we then demonstrate 25.6 Gb/s data transmission over 13.5 km SMF-28. These low-cost FP laser devices are promising candidates to provide cost-effective solutions for use in uncooled Si photonics transmitters in inter/hyper data centers and metropolitan data links.

https://doi.org/10.1364/PRJ.6.001062

1. INTRODUCTION

Monolithic integration of III-V lasers on silicon (Si) substrates has recently shown substantial advances by utilizing self-assembled quantum dots (QDs) as the active region. Their unique properties, in particular the enhanced tolerance to defects [1], have allowed rapid development in 1.3 μm InAs/GaAs QD light emitters grown directly on both offcut Si (001) substrates and on-axis Si (001) substrates, including Fabry–Perot (FP) lasers [2–5], micro-lasers [6–8], superluminescent diodes [9,10], and distributed feedback lasers [11]. The high-defect tolerance mechanism for monolithic III-V/Si integration [12,13] has meant that most research on monolithic 1.3 μm QD lasers on Si has focused on reducing defect density and enhancing static laser properties (e.g., threshold current, output power, maximum working temperature, and reliability). Other than that, for realizing practical applications in data communication systems, it is also crucial to evaluate the noise characteristics of Si-based QD lasers. The relative intensity noise (RIN), denoting the fluctuations of the output power of a semiconductor laser in its intensity, has been widely adopted as an ideal figure of merit to investigate the laser performance in fiber-optic communication networks, since the RIN leads to a limited signal-to-noise ratio (SNR) and errors, and thus an increased bit-error rate (BER) restricts the data transmission rate and distance [14].

The RIN characteristic of QD lasers on native GaAs substrates has been studied extensively [15–17] and is well understood with RIN levels as low as −160 dB/Hz obtained from InAs/GaAs QD lasers due to the unique carrier dynamics offered by the QD gain media [16]. It has been known that the RIN characteristic for QDs monolithically grown on Si substrates could not be the same as their native substrate counterparts since the defect density for QDs grown on Si is much higher when compared to that of native substrates, typically over 2×10^6 cm^{-2} compared with $\sim 1 \times 10^3$ to 1×10^4 cm^{-2} for a GaAs substrate [3,18]. And previously published QD lasers grown on Si (or Ge) substrates showed relatively diminished performance in terms of RIN. For example, by means of RIN measurements, Liu *et al.* reported a reduced optical feedback sensitivity for QD lasers grown on Si when compared with III-V quantum well lasers, and the measured RIN of the Si-based QD laser was in the range of a level between −140 and −150 dB/Hz with a defect density around 10^8 cm^{-2} [19]. In addition, the RIN of the Ge-based QD lasers has been reported to be at the level of −120 dB/Hz [20]. One of the possible reasons for the increased RIN level (in comparison with GaAs-based InAs QD lasers) could be related to the fact that the defects act as electron traps associated with defect states

and can capture or absorb carriers and photons in the laser cavity [21], which could lead to varied photon density and, thus, fluctuation of the output intensity. Therefore, an improved RIN is expected provided that the defect density can be reduced.

In this paper, by developing high-quality GaAs/Si epilayers and utilizing QDs as the active region, here, we have achieved high-performance electrically pumped continuous-wave (CW) 1.3 μm single transverse mode InAs/GaAs QD lasers directly grown on Si with threshold current as low as 12.5 mA at room temperature (RT), a maximum lasing operation temperature up to 90°C, and an ultra-low RIN measured to be in the level between −150 and −160 dB/Hz. Since our Si-based laser is designed for a Si photonics optical transmitter for low-cost data transmission in hyper/inter-data centers and metropolitan data links, on-chip QD lasers monolithically integrated with other Si-based photonic building blocks, such as modulators and waveguides, are practically susceptible to these concepts [22]. Unfortunately, such transmitters have not been realized yet. Therefore, we take the first step to evaluate the modulation characteristics of our InAs/GaAs QD lasers monolithically grown on Si by using an off-chip modulator. Attributed to this low-noise feature laser, we achieved 25.6 Gb/s data transmission over 13.5 km standard single-mode fiber (SMF-28).

2. MATERIAL GROWTH AND DEVICE FABRICATION

In this work, InAs/GaAs QD samples were directly grown on n-doped Si (001) substrates with 4° offcut toward the [011] plane by using solid source molecular beam epitaxy (MBE). The Si substrate was first thermally cleaned at 900°C for 10 min to remove the oxide layer. Numerous strategies, including an AlAs nucleation layer (NL) [3], multistep temperature growth of the GaAs buffer [23], and InGaAs/GaAs strained-layer superlattices (SLSs) [24] combined with *in situ* thermal annealing of SLSs [25], have then been employed to achieve high-quality III-V epilayers following previously optimized growth conditions [3]. Transmission electron microscopy (TEM) studies reveal that the threading dislocation density (TDD) from this optimized III-V epilayer is $<10^6$ cm^{-2}. Above the III-V buffer layers, a five-layer InAs/GaAs dot-in-a-well (DWELL) structure embedded in a GaAs/AlGaAs graded-index separated confinement heterostructure was then grown. Each DWELL layer consisted of a three-monolayer InAs QD layer sandwiched in an 8 nm $In_{0.15}Ga_{0.85}As$ quantum well (QW), which was then separated by 45 nm undoped GaAs spacer layers. More information on the epitaxial growth can be found elsewhere [3].

Figure 1(a) shows the bright-field scanning TEM image of the DWELL active region. A nearly defect-free DWELL active region is observed, suggesting that the combined strategies of an NL and SLSs with *in situ* thermal annealing have effectively suppressed the propagation of TDs into the active region. This has been further confirmed by the strong RT photoluminescence (PL) emission at ~1290 nm, which is comparable with the reference QD sample grown on native GaAs substrate, as seen from Fig. 1(b). A typical atomic force microscopy (AFM) image for an uncapped InAs QDs sample grown on a Si substrate with the same growth conditions is shown in the inset of Fig. 1(b), indicating an average dot density of ~3×10^{10} cm^{-2}.

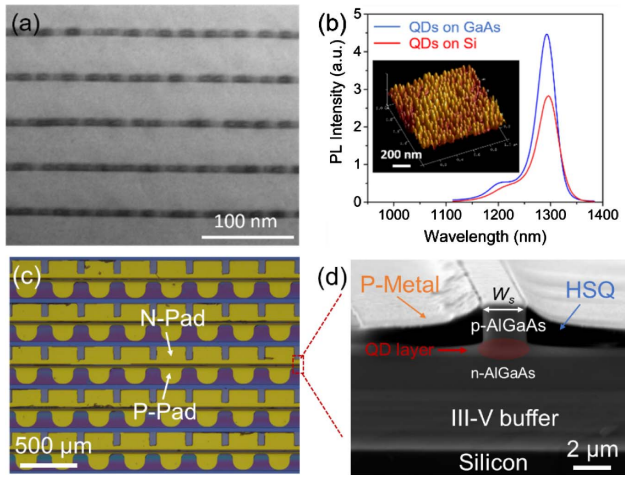

Fig. 1. (a) Bright-field scanning TEM image of the QD active layers. (b) PL comparison of InAs/GaAs QDs SLD structure grown on Si to a reference sample grown on native GaAs under the same pump conditions. The inset shows the representative AFM image of an uncapped QD sample grown on Si. (c) Optical micrography of rows of the fabricated narrow-ridge-waveguide laser. (d) Cross-sectional SEM image of the fabricated laser with as-cleaved facets.

Optical microscopy and scanning electron microscopy (SEM) images of the fabricated devices are shown in Figs. 1(c) and 1(d), respectively. Ridge waveguides with a fixed width of 2.2 μm were defined by e-beam lithography (EBL) and dry etching. SiO_2 acting as a passivation layer was used to avoid oxidation of the Al-containing layers in the air. Planarization was carried out using hydrogen silsesquioxane (HSQ) thermally cured at 180°C. Ti/Pt/Au and Au/Ge/Ni/Au metallization were used for the formation of ohmic contacts to the p+ GaAs contacting layer and the exposed n+ GaAs layer, respectively. After thinning the Si substrate to ~120 μm, the laser bars were cleaved into the desired cavity lengths with the rear facet coated with 95% high reflection (HR) coating. Laser bars were then mounted epi-side up on a copper heatsink using indium–silver low-melting-point solder and directly probed (without wire-bonding) to enable testing. Unless stated otherwise, all laser measurements were performed under CW operation at RT.

3. EXPERIMENT SETUP

A. RIN Measurement Setup

Figure 2 shows the experimental system for the RIN experiment. The 2.2 μm × 2.5 mm monolithic QD laser was

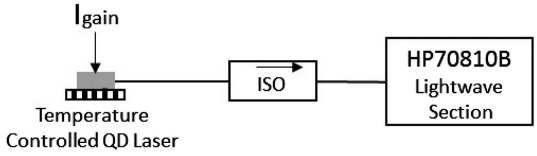

Fig. 2. Experimental setup of RIN measurement. ISO, optical isolator.

mounted on a copper heatsink and had its temperature stabilized at 25°C via a thermoelectric cooling controller. The QD laser was biased at different bias current (I_{gain}) using two electrical probes, and the laser output was coupled into the HP 70810B Lightwave Section via a lensed fiber with 1.7 μm spot size. An optical isolator with an isolation ratio of 60 dB was used to prevent any feedback into the laser cavity. The overall system noise is measured by HP 70810B, which is not only the contribution from the RIN of the laser, but also the system thermal noise and the photodetector shot noise. Thus, the RIN of the laser is calculated in HP 70810B by subtracting the contributions from the thermal noise and the shot noise from the overall measured system noise. The thermal noise is measured by turning off the light into the photodetector and by measuring the noise spectral density from the amplifier and the electronics that follows the photodetector, and this is usually constant. However, the shot noise is due to the quantum nature of light that is incident on the photodetector, it varies with the average power, and the mean square noise power is calculated from $2qI_{ph}B$, where q is the electronic charge, I_{ph} is the photocurrent, and B is the electronic bandwidth of the measurement system, typically normalized to 1 Hz.

B. Data Transmission Setup

Figure 3 shows the experimental system for the data transmission experiment. The 2.5 mm long QD laser was biased at 40 mA, emitting 6.86 dBm CW output power. Using the 1.7 μm lensed fiber, we obtained 3.66 dBm power into the SMF-28, evidencing that the primary transverse mode of our laser is the fundamental mode. The CW signal is subsequently modulated by an X-cut Mach–Zehnder modulator (MZM) biased at quadrature. The MZM was driven with a pattern generator (PG) that generates a pseudorandom bit sequence of length of $2^{15}-1$, generating a non-return-to-zero (NRZ) on–off-keying (OOK) modulated signal of 23 dB extinction ratio. The modulated signal had −2.34 dBm power and was launched into a spool of 13.5 km SMF-28 that had a dispersion of 16.5 ps/(nm · km) and a total loss of −4.2 dB. It should be noted that this 13.5 km SMF was used to comply with the IEEE 802.3 standard for the optical long reach [26].

After transmission, a variable optical attenuator (VOA) was used to change the optical power into the receiver, and the captured signal was down-sampled to one sample per symbol and then threshold-detected after clock recovery and pattern synchronization. This emulates the simplest data receiver that is widely deployed in DC interconnection [26]. Due to the limitation of the offline process, the maximum bit error rate (BER) can only be calculated from 327,670 bits.

Fig. 3. Experimental system for data transmission. PC, polarization controller; Amp., radio frequency amplifier; PPG, pseudorandom pattern generator; SMF-28, standard single-mode fiber.

4. EXPERIMENT RESULTS

A. Static Characteristics

Figure 4(a) shows the representative RT light-current-voltage (LIV) measurement of a 2.2 μm × 2.5 mm narrow-ridge-waveguide FP laser device. The turn-on voltage is 1.5 V. The measured threshold current and slope efficiency are 12.5 mA and 0.162 W/A, respectively. The single facet output power is 25 mW at 200 mA, with no obvious power saturation up to this current injection. Figure 4(b) shows the lasing intensity profiles of near-field measurement with different injection currents and the infrared (IR) camera image of a single lasing spot (inset). The spot intensity is greatest in the center and tails off at the edges, following a Gaussian profile. This profile reduces width as the threshold current is reached and maintains a single-mode profile with increasing current, which evidences the single transverse mode TME_{00} achieved by our narrow-ridge laser. A high-resolution RT lasing spectrum of the same FP device measured at 40 mA (which corresponds to 3.2 times the threshold current) is displayed in Fig. 4(c) showing few FP longitudinal modes centered at ∼1315 nm with the measured full-width of the lasing spectrum of ∼2.4 nm (at 40 mA). Modern Si electronics chips often work at 65°C or above; since our Si-based laser is designed for Si photonic data communications applications, it is vital that lasers can work at elevated temperatures up to, at least, 65°C. In this aspect, temperature-dependent light-current (L-I) characteristics of a 2.2 μm × 4 mm narrow-ridge-waveguide FP laser device were investigated under CW operation with the results shown in Fig. 4(d). As seen, the maximum heatsink temperature for maintaining ground state lasing, in this case, is 90°C. P-type modulation doping and hard soldering with better heatsink will be utilized in the future to improve the temperature characteristics of the InAs/GaAs QD laser on Si.

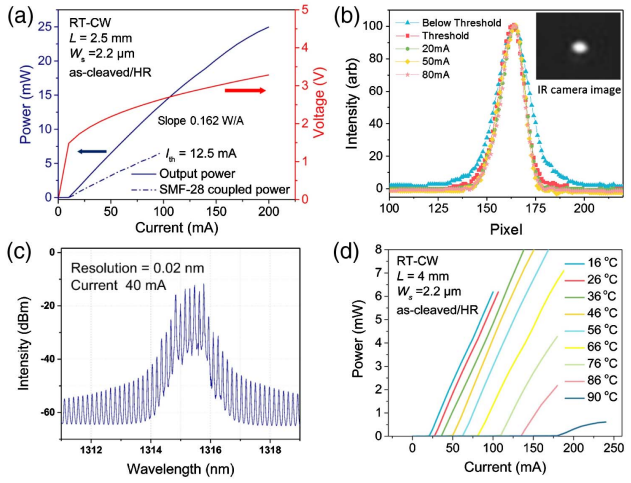

Fig. 4. (a) RT CW LIV curves for total power and single-mode coupled power from a 2.2 μm × 2.5 mm narrow-ridge-waveguide laser. (b) Lateral near-field intensity profiles with different injection currents. Inset: infrared (IR) camera image of lasing near-field at the threshold of 20 mA (well above threshold). (c) High-resolution CW lasing spectrum from a 2.2 μm × 2.5 mm narrow-ridge-waveguide laser at an injection current of 40 mA. (d) Measured CW L-I curve from a 2.2 μm × 4 mm narrow-ridge-waveguide laser as a function of temperature.

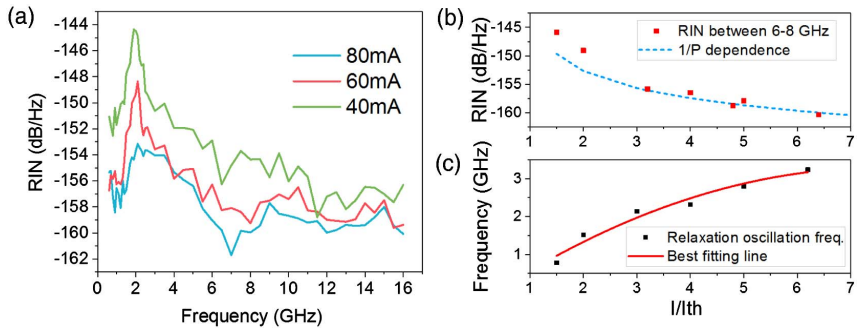

Fig. 5. (a) RIN spectra up to 16 GHz at gain currents of 40, 60, and 80 mA. (b) Measured RIN in the 6–10 GHz region with bias. (c) Relaxation oscillation frequency with bias.

B. Dynamic Characteristics

In this work, the RIN of a 2.2 μm × 2.5 mm laser was measured at varied bias points as shown in Fig. 5. The threshold current of the laser was 12.5 mA, and Fig. 5(a) shows the RIN spectra up to 16 GHz for I/I_{th} of 3.2, 4.8, and 6.4. The measured RIN is less than −150 dB/Hz when biased at gain currents greater than 60 mA ($I/I_{th} > 4.8$). At higher powers, the RIN decreases with an increase in power with a P^{-1} dependence [14] as confirmed in Fig. 5(b). However, at lower powers, it decreases with an increase in power with a P^{-3} dependence, explaining the reason for deviation at lower bias points in Fig. 5(b). Nevertheless, the measured RIN at $I/I_{th} = 1.5$ was −145.85 dB/Hz, which is comparable to the work previously reported [19]. The relaxation oscillation frequency increases from 1 to 3 GHz when the gain current is increased from 20 to 80 mA as shown in Fig. 5(c). The relatively lower bandwidth of this laser is a result of a longer photon lifetime due to its longer cavity length (2.5 mm). To achieve lasing with a shorter cavity, it could be reached by increasing either the QD density or the dot layers in the future [27,28].

Figures 6(a) and 6(b) show the eye diagrams of the received signal back-to-back, and after transmission, both measured at a received power of −7 dBm. An opened eye diagram with a Q factor of 7 was obtained at back-to-back, corresponding to a BER of about 1×10^{-12} under the assumption of Gaussian noise for both level 1 and level 0. After transmission, the dispersion inter-symbol interference (ISI) caused a thicker level 1, which reduced the Q factor to 5.

Figure 6(c) shows the measured BER as a function of the received optical power at back-to-back (open markers) and after transmission (closed markers) using hard decision. At the forward error correction threshold of 2×10^{-4}, the receiver sensitivities at back-to-back and after transmission were −11.4 dBm and −10.3 dBm, respectively. The 1.1 dB power penalty was primarily due to the impact of chromatic dispersion. As a result, we obtained loss budgets of 10 dB and 8.75 dB for the 25.6 Gb/s data communications at back-to-back and after 13.5 km fiber transmission, respectively. Received optical power has a linear relationship with $-\log_{10}$ (BER) when a signal is limited by white noise [14]. When the received optical power is below 0 dBm, the dominated noise in a direct-detection system is thermal noise, which is modeled as white noise. The linear relationship between $-\log_{10}$ (BER) and the receiver power

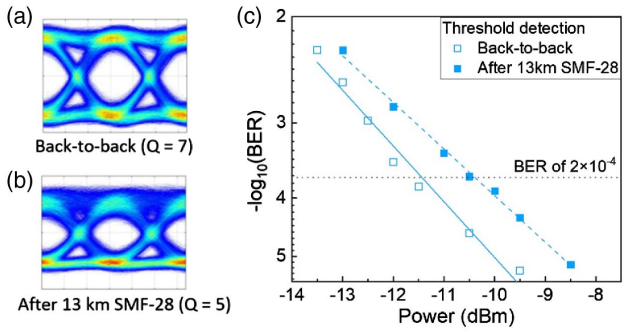

Fig. 6. (a) Experimental results. 25.6 Gb/s eye diagrams (a) at back-to-back (received power of −7 dBm) and (b) after transmission over 13 km SMF-28. (c) BER at different received power at back-to-back (square marker) and after transmission (circle marker) using threshold detection.

evidenced that the system does not have additional interference or distortion; i.e., the system is thermal-noise-limited.

5. CONCLUSION

We have demonstrated high-performance electrically pumped InAs/GaAs QD lasers monolithically grown on Si. The narrow-ridge-waveguide lasers have achieved RT CW threshold currents as low as 12.5 mA at room temperature, and operate up to 90°C. The compatible and ultra-low RIN characteristic was measured at the level of < −150 dB/Hz at frequency up to 16 GHz. Based on this low RIN, 25.6 Gb/s data transmission was obtained after transmitting over 13.5 km SMF-28. Our results show that the monolithically grown QD lasers on Si with high-performance and low-noise features are very promising for future inter-data-center interconnections.

Funding. Engineering and Physical Sciences Research Council (EPSRC) (EP/P006973/1); Royal Academy of Engineering (RF201617/16/28); Chinese Scholarship Council.

Acknowledgment. M. Liao thanks the Chinese Scholarship Council for funding her studies. S. Chen acknowledges the Royal Academy of Engineering for funding his Research Fellowship.

REFERENCES

1. A. Y. Liu, S. Srinivasan, J. Norman, A. C. Gossard, and J. E. Bowers, "Quantum dot lasers for silicon photonics [Invited]," Photon. Res. **3**, B1–B9 (2015).
2. A. Y. Liu, C. Zhang, J. Norman, A. Snyder, D. Lubyshev, J. M. Fastenau, A. W. K. Liu, A. C. Gossard, and J. E. Bowers, "High performance continuous wave 1.3 μm quantum dot lasers on silicon," Appl. Phys. Lett. **104**, 041104 (2014).
3. S. Chen, W. Li, J. Wu, Q. Jiang, M. Tang, S. Shutts, S. N. Elliott, A. Sobiesierski, A. J. Seeds, I. Ross, P. M. Smowton, and H. Liu, "Electrically pumped continuous-wave III-V quantum dot lasers on silicon," Nat. Photonics **10**, 307–311 (2016).
4. S. Chen, M. Liao, M. Tang, J. Wu, M. Martin, T. Baron, A. Seeds, and H. Liu, "Electrically pumped continuous-wave 1.3 μm InAs/GaAs quantum dot lasers monolithically grown on on-axis Si (001) substrates," Opt. Express **25**, 4632–4639 (2017).
5. D. Jung, Z. Zhang, J. Norman, R. Herrick, M. J. Kennedy, P. Patel, K. Turnlund, C. Jan, Y. Wan, A. C. Gossard, and J. E. Bowers, "Highly reliable low-threshold InAs quantum dot lasers on on-axis (001) Si with 87% injection efficiency," ACS Photon. **5**, 1094–1100 (2017).
6. Y. Wan, Q. Li, A. Y. Liu, A. C. Gossard, J. E. Bowers, E. L. Hu, and K. M. Lau, "Optically pumped 13 μm room-temperature InAs quantum-dot micro-disk lasers directly grown on (001) silicon," Opt. Lett. **41**, 1664–1667 (2016).
7. Y. Wan, J. Norman, Q. Li, M. J. Kennedy, D. Liang, C. Zhang, D. Huang, Z. Zhang, A. Y. Liu, A. Torres, D. Jung, A. C. Gossard, E. L. Hu, K. M. Lau, and J. E. Bowers, "1.3 μm submilliamp threshold quantum dot micro-lasers on Si," Optica **4**, 940–944 (2017).
8. N. Kryzhanovskaya, E. Moiseev, Y. Polubavkina, M. Maximov, M. Kulagina, S. Troshkov, Y. Zadiranov, Y. Guseva, A. Lipovskii, M. Tang, M. Liao, J. Wu, S. Chen, H. Liu, and A. Zhukov, "Heat-sink free CW operation of injection microdisk lasers grown on Si substrate with emission wavelength beyond 1.3 μm," Opt. Lett. **42**, 3319–3322 (2017).
9. S. Chen, M. Tang, Q. Jiang, J. Wu, V. Dorogan, M. Benamara, Y. Mazur, G. Salamo, P. Smowton, A. Seeds, and H. Liu, "InAs/GaAs quantum-dot superluminescent light-emitting diode monolithically grown on a Si substrate," ACS Photon. **1**, 638–642 (2014).
10. M. Liao, S. Chen, S. Huo, S. Chen, J. Wu, M. Tang, K. Kennedy, W. Li, S. Kumar, M. Martin, T. Baron, C. Jin, I. Ross, A. Seeds, and H. Liu, "Monolithically integrated electrically pumped continuous-wave III-V quantum dot light sources on silicon," IEEE J. Sel. Top. Quantum Electron. **23**, 1900910 (2017).
11. Y. Wang, S. Chen, Y. Yu, L. Zhou, L. Liu, C. Yang, M. Liao, M. Tang, Z. Liu, J. Wu, W. Li, I. Ross, A. J. Seeds, H. Liu, and S. Yu, "Monolithic quantum-dot distributed feedback laser array on silicon," Optica **5**, 528–533 (2018).
12. J. Wu, S. Chen, A. Seeds, and H. Liu, "Quantum dot optoelectronic devices: lasers, photodetectors and solar cells," J. Phys. D **48**, 363001 (2015).
13. E. Tournié, L. Cerutti, J.-B. Rodriguez, H. Liu, J. Wu, and S. Chen, "Metamorphic III–V semiconductor lasers grown on silicon," MRS Bull. **41**, 218–223 (2016).
14. G. P. Agrawal, *Fiber-Optic Communication Systems*, 4th ed. (Wiley, 2010).
15. M. Krakowski, P. Resneau, M. Calligaro, H. Liu, and M. Hopkinson, "High power, very low noise, C.W. operation of 1.32 μm quantum-dot Fabry–Perot laser diodes," in *IEEE 20th International Semiconductor Laser Conference, Conference Digest* (IEEE, 2006), pp. 39–40.
16. A. Capua, L. Rozenfeld, V. Mikhelashvili, G. Eisenstein, M. Kuntz, M. Laemmlin, and D. Bimberg, "Direct correlation between a highly damped modulation response and ultra low relative intensity noise in an InAs/GaAs quantum dot laser," Opt. Express **15**, 5388–5393 (2007).
17. A. Gubenko, I. Krestnikov, D. Livshtis, S. Mikhrin, A. Kovsh, L. West, C. Bornholdt, N. Grote, and A. Zhukov, "Error-free 10 Gbit/s transmission using individual Fabry-Perot modes of low-noise quantum-dot laser," Electron. Lett. **43**, 1430–1431 (2007).
18. M. A. Tischler, T. Katsuyama, N. A. El-Masry, and S. M. Bedair, "Defect reduction in GaAs epitaxial layers using a GaAsP-InGaAs strained-layer superlattice," Appl. Phys. Lett. **46**, 294–296 (1985).
19. A. Y. Liu, T. Komljenovic, M. L. Davenport, A. C. Gossard, and J. E. Bowers, "Reflection sensitivity of 1.3 μm quantum dot lasers epitaxially grown on silicon," Opt. Express **25**, 9535–9543 (2017).
20. Y.-G. Zhou, C. Zhou, C.-F. Cao, J.-B. Du, Q. Gong, and C. Wang, "Relative intensity noise of InAs quantum dot lasers epitaxially grown on Ge," Opt. Express **25**, 28817–28824 (2017).
21. A. Liu, R. Herrick, O. Ueda, P. Petroff, A. Gossard, and J. Bowers, "Reliability of InAs/GaAs quantum dot lasers epitaxially grown on silicon," IEEE J. Sel. Top. Quantum Electron. **21**, 1900708 (2015).
22. B. Jalali and S. Fathpour, "Silicon photonics," J. Lightwave Technol. **24**, 4600–4615 (2006).
23. M. Akiyama, Y. Kawarada, and K. Kaminishi, "Growth of single domain GaAs layer on (100)-oriented Si substrate by MOCVD," Jpn. J. Appl. Phys. **23**, L843–L845 (1984).
24. M. Tang, S. Chen, J. Wu, Q. Jiang, K. Kennedy, P. Jurczak, M. Liao, R. Beanland, A. Seeds, and H. Liu, "Optimizations of defect filter layers for 1.3-μm InAs/GaAs quantum-dot lasers monolithically grown on Si substrates," IEEE J. Sel. Top. Quantum Electron. **22**, 50–56 (2016).
25. J. R. Orchard, S. Shutts, A. Sobiesierski, J. Wu, M. Tang, S. Chen, Q. Jiang, S. Elliott, R. Beanland, H. Liu, P. M. Smowton, and D. J. Mowbray, "In situ annealing enhancement of the optical properties and laser device performance of InAs quantum dots grown on Si substrates," Opt. Express **24**, 6196–6202 (2016).
26. "IEEE P802.3ba 40 Gb/s and 100 Gb/s Ethernet task force," IEEE Std 802.3ba (2010).
27. L. F. Lester, A. Stintz, H. Li, T. C. Newell, E. A. Pease, B. A. Fuchs, and K. J. Malloy, "Optical characteristics of 1.24 μm InAs quantum-dot laser diodes," IEEE Photon. Technol. Lett. **11**, 931–933 (1999).
28. A. R. Kovsh, N. A. Maleev, A. E. Zhukov, S. S. Mikhrin, A. P. Vasil'ev, E. A. Semenova, Y. M. Shernyakov, M. V. Maximov, D. A. Livshits, V. M. Ustinov, N. N. Ledentsov, D. Bimberg, and Z. I. Alferov, "InAs/InGaAs/GaAs quantum dot lasers of 1.3 μm range with enhanced optical gain," J. Cryst. Growth **251**, 729–736 (2003).